Controlled microparticle separation using whispering gallery mode forces *

Yuhe Chang* Oleksiy Svitelskiy** Kamil L. Ekinci*,***
Sean B. Andersson*,****

- * Department of Mechanical Engineering, Boston University, Boston, MA 02215 USA (e-mail: yuhec@bu.edu).
- ** Department of Physics, Gordon College, Wenham, MA 01984 USA (e-mail: oleksiy.svitelskiy@gordon.edu))
- *** Division of Materials Science and Engineering, and the Photonics Center, Boston University, Boston, Massachusetts 02215, USA (e-mail: ekinci@bu.edu)
- **** Division of System's Engineering, Boston University, Boston, MA
 02215 USA (e-mail: sanderss@bu.edu)

Abstract: There is a wide variety of applications that require sorting and separation of microparticles from a large cluster of similar objects. Existing methods can distinguish micro-particles by their bulk properties, such as their size, density, and electric polarizability. These methods, however, are not selective with respect to the individual geometry of the particles. In this work, we focus on the use of a resonance effect between a microparticle and an evanescent light field known as the Whispering Gallery Mode (WGM) force. The WGM force is highly sensitive to the radius of the particle and is both controllable and tunable. In this paper, we explore through simulation the design of a WGM-based device for micro-particle separation. In this device, particles flow in through an inlet and are carried over two actuation regions given by waveguides carrying laser light to generate the evanescent field. Particles are observed by a camera, allowing for feedback control on the power of the lasers. While the basic control structure is simple, there are several challenges, including unknown disturbances to the fluid flow, limited laser power, and uni-directional control over each actuation region. We combine Expectation Maximization with Kalman filtering to both estimate the unknown disturbance and filter the measurements into a position estimate. We then develop simple hybrid controllers and compare them to the ideal setting (without any constraints) based on a Linear-Quadratic-Gaussian (LQG) control approach.

 $\label{lem:control} \textit{Keywords:} \ \text{Optical Implement, Optical Nonlinearities, Optical stochastic control, LQG control method$

1. INTRODUCTION

Microparticle separation refers to the general problem of selectively moving individual micrometer-sized particles based on a variety of physical properties. Applications for these techniques are widespread and can be found in, e.g., microbiology (Sajeesh and Sen, 2014; Rieseberg, 2001; Lin and Lee, 2008), pharmacology in (Toner and Irimia, 2005), biomedical engineering (Vaziri and Gopinath, 2008; Suresh et al., 2005), the electronics industry (Whitesides, 2006; Manz et al., 1992), where they are applied to sort different micron-scale particles such as cells, chromosome and chemical ions. Generally, separation and sorting techniques can be broadly categorized into either passive or active methods. (Zhu and Trung Nguyen, 2010; Sajeesh and Sen, 2014). Passive methods mainly rely on the changes in hydrodynamic effects induced by the different physical properties of the particles such as the channel geometry and inherent hydrodynamic forces (Bhagat et al., 2010).

These approaches do not require external forces and can be useful where there are strict power requirements. Active methods require an external actuation from, e.g., an electrical, magnetic, or optical field, for imparting a selective force (Kersaudy-Kerhoas et al., 2008). These techniques have relatively higher sorting sensitivity than passive approaches. In this work, we focus on an active method to sort based on the *geometry* of the particle using an optical interaction known as a Whispering Gallery Mode (WGM).

The WGM interaction is related to but distinct from the better known method of optical tweezers. Optical tweezers use a field created by a focused beam of coherent light to generate an optical force that can be used to hold and manipulate meso-scale objects (Ashkin et al., 1986; Neuman and Block, 2004; Neuman and Nagy, 2008; Molloy and Padgett, 2002) and have found broad application in biology, and the physical sciences (Curtis et al., 2002; Grier, 1997; Astratov et al., 2013). They are not inherently sensitive to particle geometry, however, and are thus limited in the precision with which they can select by geometric features such as radius or perfectness of shape.

 $^{^{\}star}$ This work was supported in part by NSF through grant CMMI-1661586 and CMMI-1661700.

The WGM is a resonance effect caused by an optical field coupling into a cavity with a smooth structure (Strutt, 2011). The specific wavelength that resonates is a function of both the geometry and the refractive index of the particle and, with a sharp resonance, is very selective with respect to that geometry. Previous work, including some by one of the authors, (Li et al., 2013; Svitelskiy et al., 2011), has shown that the WGM interaction can be generated between a tapered optical fiber and micron-scale beads, leading to directed motion of the particle along the fiber, demonstrating that his effect can be used as the basis for creating a highly selective microfluidic platform for particle separation.

In this work, we explore the design of such a platform from the control point of view. The essential idea is to flow in beads of disperse sizes and, using the WGM effect, control them to specific locations so they get collected in bins. Among the challenges for control design is that the laser power is limited and can only actuate in the direction defined by the direction of propagation of the light field. In addition, the beads are subject to both unknown disturbances (due to variations in the fluid flow carrying particles through the device) as well as random, Brownian fluctuations (due to the size scale of the particles).

The remainder of this paper is organized as follows. We begin in Sec. 2 with the necessary physical background and description of the device setup and use this in Sec. 3 to develop a discrete-time state-space model of the particle motion. To estimate the system state and the unknown disturbance, we apply a Kalman filter and the Expectation Maximization (EM) algorithm in Sec. 3.1 before turning to control design in Sec. 3.2. There we consider both the ideal setting of unlimited, bidirectional control as well as control under the more realistic constraints of the device. The approach is demonstrated through simulation in Sec. 4, before providing concluding remarks in Sec. 5.

2. PROBLEM DESCRIPTION AND SYSTEM SETUP

The basic structure of a separation device based on the WGM interaction is shown in Fig. 1. In this device, fluid flows at a constant rate from the inlet to the output, carrying particles of dispersing sizes through the system. These particles pass over two laser waveguides, each carrying a laser propagating in the direction shown. When a particle of the right geometry is over a waveguide, it will feel a force due to the WGM interaction. For simplicity, in the remainder of this article, we limit the geometry considered to spherical particles of different radii. The magnitude of the optical force depends on both the wavelength and the power of the laser. Because switching the direction of the laser requires external optomechanical hardware, we assume that the direction is fixed but that the wavelength can be adjusted (to select a specific particle size) and that the power can be varied (giving us a variable control input). On the far side of the device is an array of catch bins and the goal is to move beads of specific sizes into specific bins.

When a particle is not over a waveguide it experiences a force due to the fluid flow and, due to the micrometer scale of the particle, a random Brownian fluctuation. As illustrated in Fig. 1, the trajectory of the particle is broken

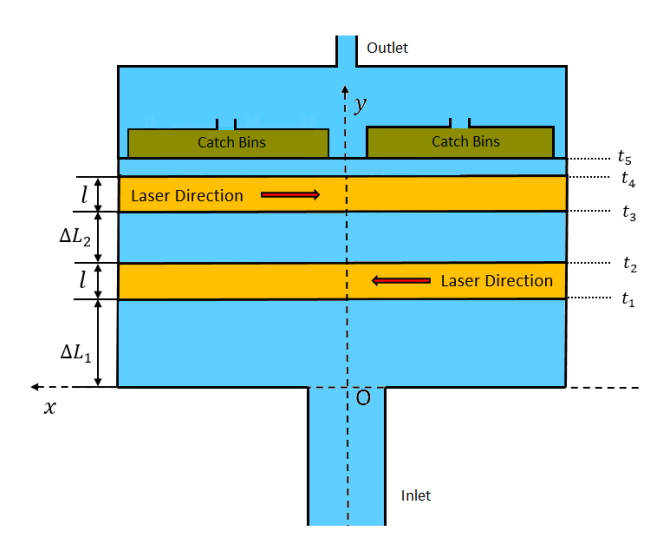


Fig. 1. Schematic of device for particle separation using the WGM interaction.

down into five regimes. The particle first flows according to the fluid motion, uncontrolled by any optical interaction. Time t_1 is defined by the moment the particle begins to cross over the first waveguide. From t_1 to t_2 (defined by when the particle leaves the first waveguide), a control force, directed only to the left, can be applied. At the time t_3 the particles move over the second waveguide and a force can be applied until time t_4 , this time directed only to the right. For ease of exposition, we assume that the distance from the end of the second waveguide to the catch bins is small enough to be ignored.

With the device structure established, we now develop the dynamic model for the particle motion. We assume that the velocity in the y direction remains constant, though since the controls developed in Sec. 3.2 depend on the observed location of the particle and not on time, this assumption is not necessary. Motion in the lateral (x) direction is determined by the particle-fluid interaction. The Reynolds number of this setup is given by

$$Re = \frac{\rho L v}{\eta},\tag{1}$$

where ρ is the density of the fluid flow, v is a typical velocity of the particle in the fluid, η is the dynamic viscosity of the fluid, and L is a typical length scale in the problem (White, 2011). Assuming the device will be operated using water at room temperature and with beads on the order of 10 μ m in diameter, the Reynolds number is in the range of $10^{-4} \sim 10^{-5}$. This implies we are operating in the Stokes' region where inertia can be ignored. The drag force experienced by the particle is then given by

$$F_{\text{Drag}} = -\gamma v = -6\pi \eta r v, \qquad (2)$$

where r is the radius of the particle, η is the dynamic viscosity, and v is the flow velocity relative to the object. Finally, the fluid flow will not be oriented perfectly from inlet to outlet. We model this by including a disturbance d. While in practice this disturbance will depend on both the location of the particle in the device and details such as particle size,, we simplify the situation here by assuming it is constant (though unknown), leading to the lateral dynamics

$$\gamma \dot{x} = F_{\text{optical}} + d + w, \tag{3}$$

where w is the process noise arising thermal fluctuations in the fluid system and $F_{optical}$ is the applied optical force. This optical force is generated by the resonant coupling of the evanescent optical field generated by the laser passing through the light guide and the particle; it is this resonance that yields the strong sensitivity to particle shape. For a spherical particle of a radius matching a resonance, the force depends on the laser power. Details on this interaction can be found Li et al. (2013); for our purposes it is enough to assume it is simply a controllable, bounded input.

To provide feedback, the device can be observed using a camera and a measurement of the position of the beads extracted using image processing algorithms (Wang et al., 2017). Because these measurements happen at discrete intervals and provide direct, though noisy, measurements of position, we can abstract the system to the discrete-time model

$$x_{k+1} = x_k + bu_k + d + w_k, (4a)$$

$$y_k = x_k + v_k, (4b)$$

where w_k is Gaussian white noise with $w_k \sim N(0, \sigma_w^2)$, v_k is Gaussian white noise with $v_k \sim N(0, \sigma_v^2)$, d is constant (but unknown), and b is selected to scale the control input so that $u_k \in \mathcal{U}(k)$ where

$$\mathcal{U}(k) = \begin{cases} [0,1], & \Delta L_1 < x_k < \Delta L_1 + l, \\ [-1,0], & \Delta L_1 + l + \Delta L_2 < x_k < \\ & \Delta L_1 + 2l + \Delta L_2, \\ 0, & \text{otherwise.} \end{cases}$$

Note that in general b may be different for each waveguide; this is a trivial modification. For simplicity of notation, we assume b is constant.

3. ESTIMATOR AND CONTROLLER DESIGN

In this section, we describe two different controllers to move beads to a desired lateral position. The first ignores all constraints and applies the Linear-Quadratic-Gaussian formulation to establish best-case performance and provide a point of comparison for the second controller. This second controller takes a practical point of view and respects the constraints, in particular the single-sided nature of the control.

In either case, a Kalman filter is used to estimate the state from the noisy measurements. In addition, as described in Sec. 3.1, either approach begins with a period where the bead is simply observed and the unknown disturbance d estimated using the Expectation-Maximization (EM) algorithm (Dempster et al., 1977).

3.1 Filtering and disturbance estimation

It is well-known that the optimal (both unbiased and minimal variance) estimator for systems of the form (4a) is a Kalman filter (Grewal and Andrews, 2014). However, to apply the Kalman filter requires knowledge of all system parameters (in this case b and the noise covariances σ_w^2 and σ_v^2 , as well as all external inputs, including the disturbance d). Since the disturbance is not known, we use the time period from the beginning until the particle passes over the first waveguide $(t_0 \text{ to } t_1)$ to jointly filter the state and estimate the disturbance by applying the EM algorithm.

The EM algorithm is an iterative technique for finding Maximum Likelihood (ML) estimates of a parameter vector. The current parameter estimate is used together with a hidden variable (here taken to be the state x_k) to form an approximation to the log-likelihood function of the parameter given the measurements. This approximation is optimized to get the next ML estimate and the process is iterated. Details on the approach can be found in, e.g., (Gibson and Ninness, 2005).

In the context of the linear system in (4a), the EM algorithm takes the form of cycling between running a Kalman filter on the data giving the current estimate of the disturbance followed by a smoother to produce distributions of the state given all the data. An estimate of the disturbance is then given by maximizing an approximation of the joint likelihood function over the state and observations. (Note that tor simplicity, in this work we omitted the smoother and worked only with the filtered state.)

The Kalman filter is a two-stage algorithm consisting of a prediction step and an update step. The prediction is given by

$$\hat{x}_{k+1|k} = \hat{x}_{k|k} + bu_k + \hat{d},\tag{5b}$$

$$P_{k+1|k} = \hat{P}_{k|k} + \sigma_w^2, \tag{5c}$$

$$\hat{x}_{k+1|k+1} = \hat{x}_{k+1|k} + K_{k+1} \left(y_k - \hat{x}_{k+1|k} \right),$$
 (5e)

$$P_{k+1|k+1} = P_{k+1|k}(1 - K_{k+1})^2 + K_{k+1}^2 \sigma_v^2,$$
 (5f)

$$P_{k+1|k+1} = P_{k+1|k} (1 - K_{k+1})^2 + K_{k+1}^2 \sigma_v^2,$$
 (5f)
$$K_k = \frac{P_{k+1|k}}{P_{k+1|k} + \sigma_v^2},$$
 (5g)

where $\hat{x}_{k+1|k}$ is the expected value of the state at time k+1 given the measurements up to time k, $P_{k+1|k}$ is the corresponding covariance, and \hat{d} is the estimate of the disturbance.

To estimate the disturbance we use the sample mean of its value, given by

$$\hat{d} = \frac{1}{N} \sum_{k=1}^{N} (\hat{x}_{k+1|k} - \hat{x}_{k|k} - bu_k), \quad N = 1, 2, 3, \dots$$
 (6)

Note that while here we only estimate the disturbance d, extending to estimate the noise parameters (σ_w^2 and σ_v^2) is straightforward.

3.2 LQG control

In the absence of any constraints, a natural choice of controller is the Linear-Quadratic-Gaussian (LQG) formulation. The LQG controller combines a Kalman filter (to estimate the state) with a Linear Quadratic Regular (LQR) feedback controller. LQR is defined by the optimization problem

$$\min_{u} \|x\|_{M_1} + \|u\|_{M_2}^2,\tag{7a}$$

subject to
$$x_{k+1} = x_k + bu_k + w_k$$
 (7b)

where x and u are the state and control signals and $\|\cdot\|_Q$ is a weighted l_2 norm. The optimal solution takes the form of a state feedback controller with

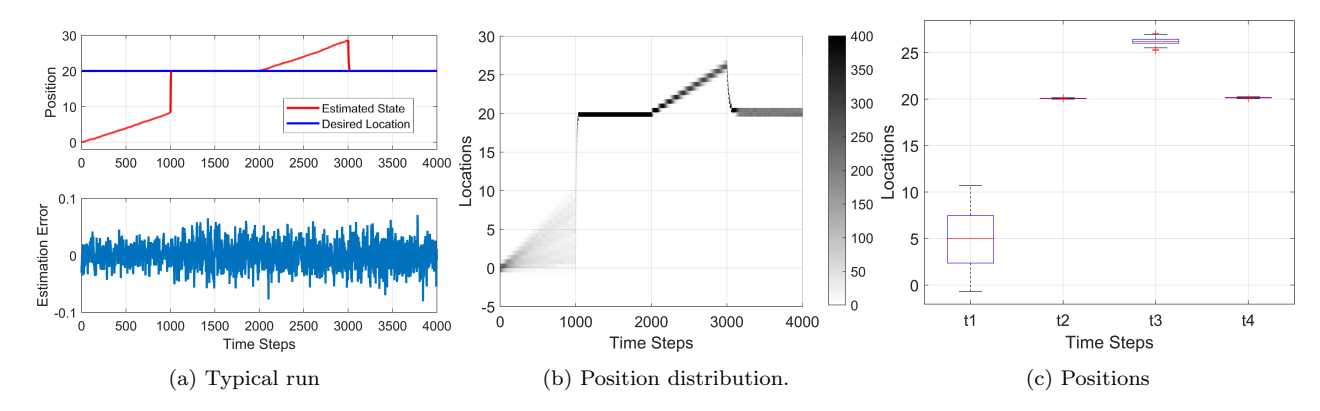


Fig. 2. LQG control. (a) The trajectory of a typical run (with disturbance d = 0.0084. (b) Particle position distribution over 400 sample runs. (c) Box plots of particle position at the start (t_1) and end (t_2) of the first actuation region and at the start (t_3) and end (t_4) of the second actuation region.

$$u_k = -K_{LQR}x_k + \tilde{r},\tag{8a}$$

$$K_{LQR} = (S + M_2)^{-1} S,$$
 (8b)

where S is the solution to the discrete-time algebraic Riccati equation and \tilde{r} is chosen to stabilize the particle at the desired location. This is then combined with the Kalman filter by replacing the true state in (8) with the current estimate \hat{x} .

One appealing feature of the LQG framework is that, assuming the initial particle location is Gaussian-distributed, the distribution on the state remains Gaussian at all times with a variance that grows when not under LQG control (in the intervals $[t_0, t_1)$ and $[t_2, t_3)$) and is reduced towards its minimum when under control (in the intervals $[t_1, t_2)$ and $[t_3, t_4)$).

3.3 Practical control

In practice, the applied control force is one-sided and bounded and thus the LQG controller described above cannot be used. We develop here an alternative controller that seeks to constantly correct for the error as much as possible within one time step, subject to the limitations of the actuators. This control law is

$$u_{k} = \begin{cases} 0, & t \in [0, t_{1}) \\ & \text{or } [t_{2}, t_{3}), \\ \max\left(\min\left(1, x_{d} - \hat{x}_{k|k} - d\right), 0\right), & t \in [t_{1}, t_{2}), \\ \min\left(\max\left(-1, x_{d} - \hat{x}_{k|k} - d\right), 0\right), & t \in [t_{3}, t_{4}) \end{cases}$$

$$(9)$$

As (9) represents a nonlinear control law, the resulting distribution of the state will no longer be Gaussian. In particular, due to the one-sided nature of the control, it is expected that the distributions at time t_2 and t_4 will have heavy tails in the uncontrolled direction.

4. SIMULATIONS AND RESULTS

To demonstrate our approach we performed 400 simulation runs. In each run, the desired location was set to $x_d = 20$ (arbitrary units of length), the process noise covariance was set to $\sigma_w^2 = 0.01$ (length²), and the measurement noise to $\sigma_v^2 = 0.04$ (length²). The disturbance for each run was selected at random from a uniform distribution on

 $[0, 10^{-2}]$, selected based on intuition that the disturbance should be small relative to the achievable control force. The total time was set to 4000 time steps (in arbitrary time units) and the times t_i evenly placed over that time interval. The error of the EM-based estimate of the disturbance using measurements from the first 1000 steps was approximately $-2.02 \times 10^{-6} \pm 3.30 \times 10^{-4}$ (length). The initial state x_0 is set to follow a normal distribution with zero mean and a covariance of 0.25 (length²).

4.1 LQG controller

A typical run under the LQG controller is shown in Fig. 2a under a drift value of 0.0084. The upper plot shows the filtered state estimate (red) and the desired location (blue) while the bottom plot shows the estimation error over the run. The LQG controller engages at time 1000, immediately bringing the particle to the target position and holds it there until it leaves the actuation region at time 2000. Drift (with a small amount of Brownian motion) then drives it until it reaches the second actuation region at time 3000 where the controller once again snaps the particle back to the desired location and holds it there until the end.

The results of all 400 runs are shown as histograms in Fig 2b. These histograms clearly show the Gaussian nature of the distribution at every point in time. The distribution is tightly centered on the desired location during both the actuation periods but then drifts (due to the disturbance) and grows in variance (due to the process noise) during the non-actuated periods. This is highlighted in the box plots in Fig. 2c which shows the particle distributions at the key points t_1 (start of the first actuation region), t_2 (end of that region), t_3 (start of the second actuation region) and t_4 (end of that region).

4.2 Practical Control

A typical run under the practical controller of (9) with a disturbance value of 0.0045 is shown in Fig. 3a. As with the LQG controller, the particle is brought right to the desired location when the first actuation region is reached. However, due to the one-sided nature of the control, the particle is now free to wander to lateral positions greater than x_d . In essence, the control enforces a lower boundary

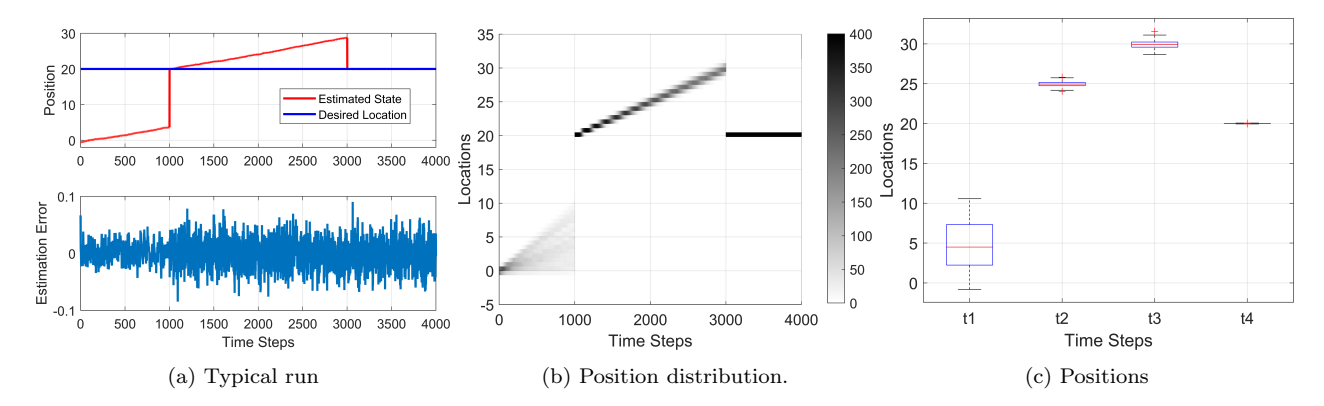


Fig. 3. Practical control. (a) The trajectory of a typical run (with disturbance d = 0.0045. (b) Particle position distribution over 400 sample runs. (c) Box plots of particle position at the start (t_1) and end (t_2) of the first actuation region and at the start (t_3) and end (t_4) of the second actuation region.

on the particle which is otherwise free to drift and diffuse. Similarly, when the particle reaches the second actuation region, the control enforces an upper boundary. Note that due to the sign of the drift, the particle is essentially pinned at the desired location during the second actuation region.

The results of all 400 runs are shown as histograms in Fig. 3a. Until time $t=t_1=1000$ the particle distribution remains Gaussian. Since the drift due to the disturbance dominates, after time t_1 , the distribution quickly drifts away from the lower boundary and begins to spread due to the process noise, maintaining its primarily Gaussian shape. Note that if the process noise dominated, the imposition of the lower boundary would lead to a non-Gaussian distribution. As with the LQG setting, the second actuation region essentially pins the particle against the upper boundary. While the particle is free to wander below due to the one-sided nature of the control, the positive drift eliminates much of that motion.

4.3 Discussion

These results show that the practical controller, despite its limitations, can be an effective approach for particle steering. In any device, it will be important to minimize the distance between the actuation regions and the total transition time to minimize the effect of the process noise.

A typical length scale of these devices is on the order of microns, implying that the process noise variance considered was on the order of 0.01 μm^2 . In practice, this value can be estimated from

$$\sigma_w^2 = 2D\Delta t,$$

where Δt is the time step and D is the diffusion coefficient, given by the Stokes-Einstein relation,

$$D = \frac{k_B T}{6\pi \eta r},$$

where k_B is the Boltzmann constant, η is the dynamic viscosity, and r is the radius of the particle. Given a particle size on the order of 10 μ m, operating in the water, and a time step on the order of 10 ms, a typical process noise variance is on the order of 10^{-5} μ m². The primary noise source is then the observation noise from the camerabased localization and the practical control is likely to be effective.

While practical experiments are likely to involve small σ_w^2 , the limitations of the practical control are more easily viewed with larger process noise. To demonstrate this we ran additional simulations with $\sigma_n^2 = 0.25$ (with all other parameters unchanged). A typical run is shown in Fig. 4b where the process noise clearly dominates. The "pinning" action of the one-sided control is best seen in the last actuation region.

The histograms over all 400 simulation runs are shown in Fig. 4b. The large process noise leads to the very rapid dispersion of the particles when uncontrolled and a clearly non-Gaussian distribution over the last 1000 time steps. This is highlighted in Fig. 4c where the box plots at the same four key times are shown.

5. CONCLUSION

This paper described and investigated a possible device for the separation of micro-scale particles based on geometric properties using Whispering Gallery Mode forces. A practical control scheme was introduced and its performance compared through simulation to an ideal setting based on an LQG controller.

Ongoing and future work involves supporting these simulation studies with experimental data to verify simulation parameters and then to demonstrate the controller in a physical setting.

REFERENCES

Ashkin, A., Dziedzic, J.M., Bjorkholm, J.E., and Chu, S. (1986). Observation of a single-beam gradient force optical trap for dielectric particles. *Opt. Lett.*, 11(5), 288–290.

Astratov, V.N., Li, Y., Svitelskiy, O.V., Maslov, A.V., Bakunov, M.I., Carnegie, D., and Rafailov, E. (2013). Microspherical photonics: Ultra-high resonant propulsion forces. *Opt. Photon. News*, 24(12), 40–40. doi:10. 1364/OPN.24.12.000040. URL http://www.osa-opn.org/abstract.cfm?URI=opn-24-12-40.

Bhagat, A.A.S., Bow, H., Hou, H.W., Tan, S.J., Han, J., and Lim, C.T. (2010). Microfluidics for cell separation. *Medical & Biological Engineering & Computing*, 48(10), 999–1014.

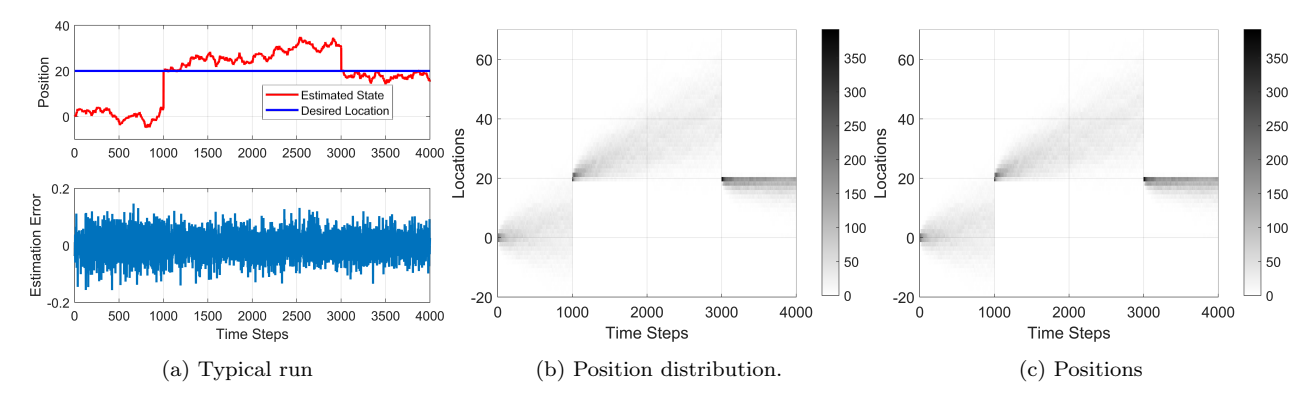


Fig. 4. Practical control with large process noise. (a) The trajectory of a typical run (with disturbance d = 0.0035. (b) Particle position distribution over 400 sample runs. (c) Box plots of particle position at the start (t_1) and end (t_2) of the first actuation region and at the start (t_3) and end (t_4) of the second actuation region.

Curtis, J.E., Koss, B.A., and Grier, D.G. (2002). Dynamic holographic optical tweezers. *Optics Communications*, 207(1), 169 – 175.

Dempster, A.P., Laird, N.M., and Rubin, D.B. (1977). Maximum likelihood from incomplete data via the EM algorithm. *Journal of the Royal statistical Society*, 39(1), 1–38.

Gibson, S. and Ninness, B. (2005). Robust maximum-likelihood estimation of multivariable dynamic systems. *Automatica*, 41(10), 1667–1682.

Grewal, M.S. and Andrews, A.P. (2014). Kalman Filtering: Theory and Practice with MATLAB. Wiley-IEEE Press, 4th edition.

Grier, D.G. (1997). Optical tweezers in colloid and interface science. Current Opinion in Colloid And Interface Science, 2(3), 264 – 270.

Kersaudy-Kerhoas, M., Dhariwal, R., and Desmulliez, M. (2008). Recent advances in microparticle continuous separation. *IET Nanobiotechnology*, 2, 1–13.

Li, Y., Maslov, A.V., Svitelskiy, O.V., Carnegie, D., Rafailov, E., and Astratov, V.N. (2013). Giant resonant light forces in microspherical photonics. In *CLEO*: 2013, CW3F.6. Optical Society of America.

Lin, Y.H. and Lee, G.B. (2008). Optically induced flow cytometry for continuous microparticle counting and sorting. *Biosensors and Bioelectronics*, 24(4), 572 – 578.

Manz, A., Harrison, D., Verpoorte, E.M., Fettinger, J.C., Paulus, A., Lüdi, H., and Widmer, H.M. (1992). Planar chips technology for miniaturization and integration of separation techniques into monitoring systems: Capillary electrophoresis on a chip. *Journal of Chromatography A*, 593(1), 253 – 258.

Molloy, J.E. and Padgett, M.J. (2002). Lights, action: Optical tweezers. *Contemporary Physics*, 43(4), 241–258.

Neuman, K.C. and Block, S.M. (2004). Optical trapping. Review of Scientific Instruments, 75(9), 2787–2809.

Neuman, K.C. and Nagy, A. (2008). Single-molecule force spectroscopy: Optical tweezers, magnetic tweezers and atomic force microscopy.

Rieseberg, L.H. (2001). Chromosomal rearrangements and speciation. *Trends in Ecology and Evolution*, 16(7), 351 – 358.

Sajeesh, P. and Sen, A.K. (2014). Particle separation and sorting in microfluidic devices: a review. *Microfluidics and Nanofluidics*, 17(1), 1–52.

Strutt, J.W. (2011). The Theory of Sound, volume 1 of Cambridge Library Collection - Physical Sciences. Cambridge University Press.

Suresh, S., Spatz, J., Mills, J., Micoulet, A., Dao, M., Lim, C., Beil, M., and Seufferlein, T. (2005). Connections between single-cell biomechanics and human disease states: gastrointestinal cancer and malaria. *Acta Biomaterialia*, 1(1), 15 – 30.

Svitelskiy, O., Sun, D., Darafsheh, A., Sumetsky, M., Lupu, A., Tchernycheva, M., and Astratov, V. (2011). Characterization of high index microsphere resonators in fiber-integrated microfluidic platforms. *Proc SPIE*, 7913, 791314.

Toner, M. and Irimia, D. (2005). Blood-on-a-chip. Annual Review of Biomedical Engineering, 7(1), 77–103.

Vaziri, A. and Gopinath, A. (2008). Cell and biomolecular mechanics in silico. *Nature materials*, 7, 15–23.

Wang, Y., Li, X., Bi, S., Zhu, X., and Liu, J. (2017). 3D micro-particle image modeling and its application in measurement resolution investigation for visual sensing based axial localization in an optical microscope. Measurement Science and Technology, 28.

White, F. (2011). *Fluid Mechanics*. McGraw-Hill series in Mechanical Engineering. McGraw Hill.

Whitesides, G.M. (2006). The origins and the future of microfluidics.

Zhu, G. and Trung Nguyen, N. (2010). Particle sorting in microfluidic systems. *Micro and Nanosystems*, 2(3), 202–216.